

## Unusually High Differential Attenuation at C Band: Results from a Two-Year Analysis of the French Trappes Polarimetric Radar Data

PIERRE TABARY AND GIANFRANCO VULPIANI

*Direction des Systèmes d'Observation, Météo France, Toulouse, France*

JONATHAN J. GOURLEY

*NOAA/National Severe Storms Laboratory, Norman, Oklahoma*

ANTHONY J. ILLINGWORTH AND ROBERT J. THOMPSON

*University of Reading, Reading, United Kingdom*

OLIVIER BOUSQUET

*CNRM/GAME, Météo France, Toulouse, France*

(Manuscript received 14 May 2008, in final form 1 April 2009)

### ABSTRACT

The differential phase ( $\Phi_{DP}$ ) measured by polarimetric radars is recognized to be a very good indicator of the path integrated by rain. Moreover, if a linear relationship is assumed between the specific differential phase ( $K_{DP}$ ) and the specific attenuation ( $A_H$ ) and specific differential attenuation ( $A_{DP}$ ), then attenuation can easily be corrected. The coefficients of proportionality,  $\gamma_H$  and  $\gamma_{DP}$ , are, however, known to be dependent in rain upon drop temperature, drop shapes, drop size distribution, and the presence of large drops causing Mie scattering. In this paper, the authors extensively apply a physically based method, often referred to as the “Smyth and Illingworth constraint,” which uses the constraint that the value of the differential reflectivity  $Z_{DR}$  on the far side of the storm should be low to retrieve the  $\gamma_{DP}$  coefficient. More than 30 convective episodes observed by the French operational C-band polarimetric Trappes radar during two summers (2005 and 2006) are used to document the variability of  $\gamma_{DP}$  with respect to the intrinsic three-dimensional characteristics of the attenuating cells. The Smyth and Illingworth constraint could be applied to only 20% of all attenuated rays of the 2-yr dataset so it cannot be considered the unique solution for attenuation correction in an operational setting but is useful for characterizing the properties of the strongly attenuating cells. The range of variation of  $\gamma_{DP}$  is shown to be extremely large, with minimal, maximal, and mean values being, respectively, equal to 0.01, 0.11, and 0.025 dB °<sup>-1</sup>. Coefficient  $\gamma_{DP}$  appears to be almost linearly correlated with the horizontal reflectivity ( $Z_H$ ), differential reflectivity ( $Z_{DR}$ ), and specific differential phase ( $K_{DP}$ ) and correlation coefficient ( $\rho_{HV}$ ) of the attenuating cells. The temperature effect is negligible with respect to that of the microphysical properties of the attenuating cells. Unusually large values of  $\gamma_{DP}$ , above 0.06 dB °<sup>-1</sup>, often referred to as “hot spots,” are reported for 15%—a nonnegligible figure—of the rays presenting a significant total differential phase shift ( $\Delta\phi_{DP} > 30^\circ$ ). The corresponding strongly attenuating cells are shown to have extremely high  $Z_{DR}$  (above 4 dB) and  $Z_H$  (above 55 dBZ), very low  $\rho_{HV}$  (below 0.94), and high  $K_{DP}$  (above 4° km<sup>-1</sup>). Analysis of 4 yr of observed raindrop spectra does not reproduce such low values of  $\rho_{HV}$ , suggesting that (wet) ice is likely to be present in the precipitation medium and responsible for the attenuation and high phase shifts. Furthermore, if melting ice is responsible for the high phase shifts, this suggests that  $K_{DP}$  may not be uniquely related to rainfall rate but can result from the presence of wet ice. This hypothesis is supported by the analysis of the vertical profiles of horizontal reflectivity and the values of conventional probability of hail indexes.

---

*Corresponding author address:* Dr. Pierre Tabary, Centre de Météorologie Radar, Direction des Systèmes d'Observation, Météo France, 42 Ave. Coriolis, 31057 Toulouse, France.  
E-mail: pierre.tabary@meteo.fr

DOI: 10.1175/2009JAMC2039.1

## 1. Introduction

Attenuation by rain may be a serious source of errors when estimating rainfall rates with C-band and X-band radars. Iterative approaches based on horizontal reflectivity ( $Z_H$ ) have only been proposed (Hitschfeld and Bordan 1954) but they are known to be unstable due to miscalibration of the radar and/or inadequacy of the assumed drop size distribution (DSD). The advent of dual polarization clearly offers new perspectives in this respect. Theoretical works [see the comprehensive review in Bringi and Chandrasekar (2001)] and observations (e.g., Carey et al. 2000; Gourley et al. 2006b, hereafter referred to as G06) suggest that the relationships between specific differential phase ( $K_{DP}$ ) and specific attenuation and specific differential attenuation ( $A_H$  and  $A_{DP}$ , respectively) are almost linear in rain at C band:

$$A_H = \gamma_H K_{DP} \quad \text{and} \quad (1)$$

$$A_{DP} = \gamma_{DP} K_{DP}, \quad (2)$$

where  $A_H$  and  $A_{DP}$  are expressed in decibels per kilometer,  $\gamma_H$  and  $\gamma_{DP}$  in decibels per degree, and  $K_{DP}$  in degrees per kilometer. The coefficients of proportionality, denoted by  $\gamma_H$  and  $\gamma_{DP}$  in (1) and (2), are, however, known to be dependent in rain upon the temperature, drop shape (oblateness), and DSD characteristics of the attenuating cells with Carey et al. (2000) quoting a typical range for  $\gamma_H$  of 0.05–0.11 dB °<sup>-1</sup> and for  $\gamma_{DP}$  of 0.01–0.03 dB °<sup>-1</sup>. Ryzhkov and Zrnić (1995) found that both coefficients increase because of Mie scattering by the larger drops at S band. Keenan et al. (2001) drew attention to the effect of the large drops on the attenuation coefficients at C band, while Carey et al. (2000) showed that at C band this effect became important once  $Z_{DR} > 2$  dB. G06 have proposed an empirical method to objectively build the curves of path integrated attenuation (PIA) =  $f(\Phi_{DP})$  and path integrated differential attenuation (PIDA) =  $g(\Phi_{DP})$ . In their Fig. 2, G06 present the results obtained for seven cases of intense convection observed by the French operational C-band polarimetric radar located in Trappes near Paris (Gourley et al. 2006a). All curves are remarkably linear and within the expected theoretical bounds but their slopes [i.e., the  $\gamma_H$  and  $\gamma_{DP}$  of (1) and (2)] appear to be variable from episode to episode. G06 tried to relate the variability of  $\gamma_H$  and  $\gamma_{DP}$  to characteristics of the attenuating cells, such as drop temperature and percentage of cells containing large diameter drops leading to Mie scattering at C band. Mie scattering effects were assumed when the percentage of attenuating cells with  $3 < Z_{DR} < 5$  dB became  $> 15\%$ . In this paper, we propose to revisit that empirical stratification

for  $\gamma_{DP}$  only using a physically based approach for determining intrinsic  $Z_{DR}$  in the stratiform region behind convective cells (Smyth and Illingworth 1998) to provide an estimate for the value of PIDA. The analysis is carried out using the same French C-band operational polarimetric radar as in G06.

## 2. Data and methodology

### a. Step-by-step description of the methodology

Smyth and Illingworth (1998) suggested using a “ $Z_{DR} \approx 0$  constraint” in the stratiform region behind convective cells to estimate the PIDA and correct radar measurements for differential attenuation. The stratiform region is defined as a low-reflectivity region where the differential phase plateaus. This constraint cannot be used for an operational algorithm because it is not always possible to find such a region for each ray. This limitation is not a problem for the present work since we are essentially interested in characterizing the  $\gamma_{DP}$  variability and we can afford not to process the unsuitable rays. The application of the “Smyth and Illingworth constraint” (hereinafter referred to as the S&I constraint) is done as follows:

- Select all rays that have at least 30° of differential phase shift ( $\Delta\Phi_{DP}$ ). This threshold value is justified in the following.
- Correct the polarimetric measurements for low signal-to-noise ratio (SNR) biases, nonmeteorological echoes, calibration biases, azimuthal interferences, and differential phase aliasing and offsets (Gourley et al. 2006a).
- Filter  $\Phi_{DP}$  and estimate  $K_{DP}$ . In the present analysis, we simply use a running, centered, median filter of length 1.68 km, corresponding to seven 240-m gates. At least 50% of the  $\Phi_{DP}$  measurements have to be available (i.e., classified as precipitation) within the filtering window to validate the  $K_{DP}$  estimate. Otherwise, the  $K_{DP}$  estimate is set to a missing value. The rather short path over which  $K_{DP}$  is estimated is related to the fact that  $K_{DP}$  will essentially be used in convective rain.
- Correct  $Z_H$  for PIA using  $\Phi_{DP}$  assuming a given  $\gamma_H$ :

$$Z_{H,\text{corrected}} = Z_{H,\text{measured}} + \gamma_H \Phi_{DP}. \quad (3)$$

Actually, as explained below, the choice of  $\gamma_H$  is coupled with the  $\gamma_{DP}$  estimation.

- For each selected ray, search for light, stratiform precipitation in regions behind convective cells from the radar’s vantage point. A so-called stratiform region is defined in this study as a series of at least 20

consecutive 240-m gates below the freezing level with (corrected) horizontal reflectivity less than 45 dBZ and no differential phase shift. The freezing-level height is retrieved from the brightband identification technique proposed by Tabary et al. (2006). The standard deviation of the differential phase ( $\Phi_{DP}$ ) over the 20 gates also has to be less than  $5^\circ$  [i.e., slightly more than the typical gate-by-gate noise found with the Trappes radar differential phase measurements in Gourley et al. (2006a)]. That value was determined subjectively by examining a large number of profiles. A stratiform region is more simply identified as a smooth plateau on the  $\Phi_{DP}$  profile.

- If the intrinsic horizontal reflectivity ( $Z_{H,intrinsic}$ ) is known, then the intrinsic  $Z_{DR,intrinsic}$  can be obtained using an empirical relationship. For instance, Bringi et al. (2001) have proposed the following formula:

$$Z_{DR,intrinsic} \text{ (dB)} = 0.048Z_{H,intrinsic} \text{ (dBZ)} - 0.774$$

if  $Z_{H,intrinsic} > 20$  dBZ, (4)

$$Z_{DR,intrinsic} \text{ (dB)} = 0 \quad \text{if} \quad Z_{H,intrinsic} < 20 \text{ dBZ.} \quad (5)$$

Figure 1 helps to assess the relevance of (4) and (5). The data have been obtained from a large number of close-range, nonattenuated, nonshielded, high-SNR data in rain collected by the French polarimetric operational Trappes radar [see Gourley et al. (2006a) for a thorough evaluation of its quality]. The mean  $Z_{DR}$  and its standard deviation have been computed for each 1-dBZ class of  $Z_H$  ranging from 0 up to 45 dBZ. The Bringi et al. (2001) model [(3) and (4) above] has been superimposed (diamonds). The agreement is remarkable even though the model tends to overestimate the intrinsic  $Z_{DR}$  by around 0.1 dB for  $Z_H$  between 15 and 20 dBZ and to underestimate it by the same amount (0.1 dB) for  $Z_H$  between 40 and 45 dBZ. For the present analysis, a linear-by-part model was fitted to the empirical data. It has been represented by a light straight line on Fig. 1. Here are the corresponding relationships:

$$Z_{DR,intrinsic} \text{ (dB)} = 0 \quad \text{if} \quad Z_{H,intrinsic} < 10 \text{ dBZ,} \quad (6)$$

$$Z_{DR,intrinsic} \text{ (dB)} = \frac{0.15(Z_{H,intrinsic} - 10)}{10}$$

if  $10 < Z_{H,intrinsic} < 20$  dBZ, (7)

$$Z_{DR,intrinsic} \text{ (dB)} = 0.15 + \frac{0.45(Z_{H,intrinsic} - 20)}{10}$$

if  $20 < Z_{H,intrinsic} < 30$  dBZ, (8)

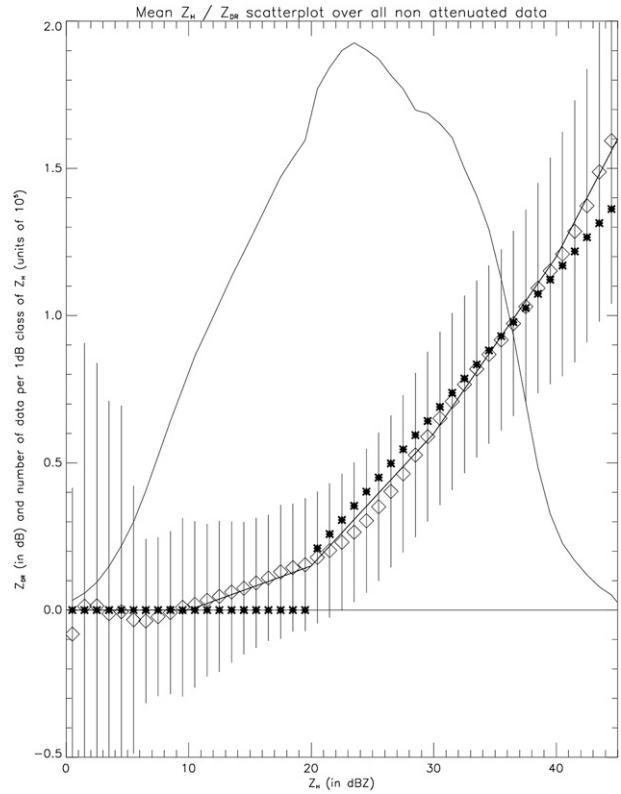


FIG. 1. Empirical ( $Z_H$ ,  $Z_{DR}$ ) scatterplot. The mean (diamond)  $\pm$  std dev of  $Z_{DR}$  has been computed for each class of  $Z_H$ . The bin size for  $Z_H$  was 1 dBZ. The Bringi et al. (2001) simplified relationship (crosses) and the linear-by-part fitted model used in the analysis (light straight line) have been superimposed. Also shown is the number of data used for each class of  $Z_H$ . Notice that for that variable the vertical scale is expressed in  $10^5$  units.

$$Z_{DR,intrinsic} \text{ (dB)} = 0.6 + \frac{0.6(Z_{H,intrinsic} - 30)}{10}$$

if  $30 < Z_{H,intrinsic} < 40$  dBZ, (9)

$$Z_{DR,intrinsic} \text{ (dB)} = 1.2 + \frac{0.4(Z_{H,intrinsic} - 40)}{5}$$

if  $40 < Z_{H,intrinsic} < 45$  dBZ. (10)

Figure 1 also helps in setting the minimum value  $\Delta\Phi_{DP}$  required in the first step of the processing (first item above). The scatter of the intrinsic  $Z_{DR}$  ( $Z_{DR,intrinsic}$ ) around the linear-by-part fitted model is typically  $\pm 0.2$  dB. If we assume a typical  $\gamma_{DP}$  value of  $0.03 \text{ dB}^{-1}$ , then a  $30^\circ$  differential phase shift (which is the value that was retained) corresponds to a PIDA of about 1 dB, which is 5 times larger than the uncertainty on the intrinsic  $Z_{DR}$ . As a consequence, setting  $\Delta\Phi_{DP}$  to  $30^\circ$  guarantees that the  $\gamma_{DP}$  estimation has a precision better than 20%.

- Once the intrinsic differential reflectivity ( $Z_{DR,intrinsic}$ ) is estimated for each of the 20 gates, then the simple arithmetic mean is taken ( $Z_{DR,intrinsic,mean}$ ) and the slope  $\gamma_{DP}$  can be computed as follows:

$$\gamma_{DP} = \frac{(Z_{DR,intrinsic,mean} - Z_{DR,measured})}{\Phi_{DP}}. \quad (11)$$

If the  $\gamma_H$  value assumed initially to correct horizontal reflectivity measurements was not adequate, then the intrinsic  $Z_{DR,intrinsic}$  and, subsequently, the  $\gamma_{DP}$  estimation may be biased. In the appendix, however, we show that given the typical range of variation of  $\gamma_H$  (between 0.07 and 0.13 dB °<sup>-1</sup>) the relative error on the estimated  $\gamma_{DP}$  is around 5%. Even though that amount of error may be considered to be fairly acceptable, a refinement has been introduced to solve for  $\gamma_H$  and  $\gamma_{DP}$  simultaneously. The approach relies on the assumption that  $\gamma_H$  and  $\gamma_{DP}$  are proportional in rain. Using numerical simulations, Vulpiani et al. (2008) have shown that the following relationship (see their Fig. 1),

$$\gamma_{DP} = 0.3\gamma_H, \quad (12)$$

was fairly stable for a large range of temperatures,  $N_W$ ,  $\mu$ , and  $D_0$ . Later we will present an analysis of 4 yr of observed raindrop spectra that supports this relationship. Similarly, G06 have empirically found ratios  $\gamma_{DP}/\gamma_H$  equal to 0.37, 0.27, 0.5, 0.34, 0.42, 0.46, and 0.56 (their Table 1). Those results reveal some variability but part of this variability is due to the uncertainty in the estimated  $\gamma_{DP}$  and even more  $\gamma_H$  and also to the fact that hail is likely to be present in several of the situations analyzed by G06. The proposed iterative approach assumes an initial value for  $\gamma_H$  (say  $\gamma_{H0}$ ), corrects  $Z_H$  for attenuation using (3), estimates the intrinsic  $Z_{DR,intrinsic}$  via (6)–(10), retrieves  $\gamma_{DP}$  with (11), and finally computes a new  $\gamma_H$  with (12). Convergence is achieved when two successive values of  $\gamma_H$  differ by less than 0.01 dB °<sup>-1</sup>. Because of the nonlinear form of the ( $Z_H$ ,  $Z_{DR}$ ) relationship [(6)–(10)], the solution for  $\gamma_H$  and  $\gamma_{DP}$  cannot be obtained in one step. In the coupled retrieval, which relies on the important assumption that precipitation is pure rain, unusually large retrieved  $\gamma_{DP}$  will be translated into unusually large  $\gamma_H$ . In this example, if the coupling is deactivated and a climatological  $\gamma_H$  value ( $\gamma_{H0} = 0.1$  dB °<sup>-1</sup>) is used, then  $Z_H$  and subsequently  $Z_{DR}$  [(6)–(10)] values in the stratiform region will be underestimated and the  $\gamma_{DP}$  estimation will be biased negatively. The impact of using or not using a coupling between  $\gamma_H$  and  $\gamma_{DP}$  will be presented and discussed in section 3.

- Once the optimal  $\gamma_H$  and  $\gamma_{DP}$  have been retrieved, all  $Z_H$  and  $Z_{DR}$  measurements along the ray between the radar and the stratiform region are corrected for attenuation using filtered  $\Phi_{DP}$ .
- Finally, the characteristics of the attenuating cells are extracted using weighted averages of the various relevant parameters ( $Z_H$ ,  $Z_{DR}$ ,  $\rho_{HV}$ ,  $K_{DP}$ , and  $T$ ), the weights being the attenuation-corrected  $Z_H$  values (expressed in linear units) at each gate:

$$Z_H^{attenuating\_cells} = \frac{\sum_{radar \rightarrow stratiform\_region} z_H Z_H}{\sum_{radar \rightarrow stratiform\_region} z_H}, \quad (13)$$

$$Z_{DR}^{attenuating\_cells} = \frac{\sum_{radar \rightarrow stratiform\_region} z_H Z_{DR}}{\sum_{radar \rightarrow stratiform\_region} z_H}, \quad (14)$$

$$\rho_{HV}^{attenuating\_cells} = \frac{\sum_{radar \rightarrow stratiform\_region} z_H \rho_{HV}}{\sum_{radar \rightarrow stratiform\_region} z_H}, \quad (15)$$

$$K_{DP}^{attenuating\_cells} = \frac{\sum_{radar \rightarrow stratiform\_region} z_H K_{DP}}{\sum_{radar \rightarrow stratiform\_region} z_H}, \quad (16)$$

$$T^{attenuating\_cells} = \frac{\sum_{radar \rightarrow stratiform\_region} z_H T}{\sum_{radar \rightarrow stratiform\_region} z_H}. \quad (17)$$

In (13)–(17),  $z_H$  is equal to  $10^{Z_H/10}$  and  $Z_H$  is the attenuation-corrected horizontal reflectivity (dBZ). The summation symbols in (13)–(17) (i.e.,  $\sum_{radar \rightarrow stratiform\_region}$ ) simply mean integration over all gates along the ray between the radar and the stratiform region through the convective cells. To extract the characteristics of the attenuating cells, the proper weights to use in (13)–(17) should be the specific differential attenuation ( $A_{DP}$ ) or the specific attenuation ( $A_H$ ) both expressed in decibels per kilogram. Those two quantities, however, are not known so we use linear horizontal reflectivity (mm<sup>6</sup> m<sup>-3</sup>) as a proxy [as in Ryzhkov et al. (2007)]. Notice that in rain, the relationship between linear horizontal reflectivity and specific attenuation is close to linear (see Table 1 of Testud et al. 2000). The temperature profile has been reconstructed under the assumption of a constant  $-6.5^\circ$  km<sup>-1</sup> lapse rate from the freezing-level height retrieved by the brightband identification algorithm (Tabary et al. 2006). Even though this is rarely alluded to, one has to concede that it is extremely difficult to obtain a very accurate estimation of the droplets' temperature inside the attenuating cells because it is highly variable in space and time and may differ significantly from ambient air temperatures. The space-time resolution of the radiosonde data is clearly not

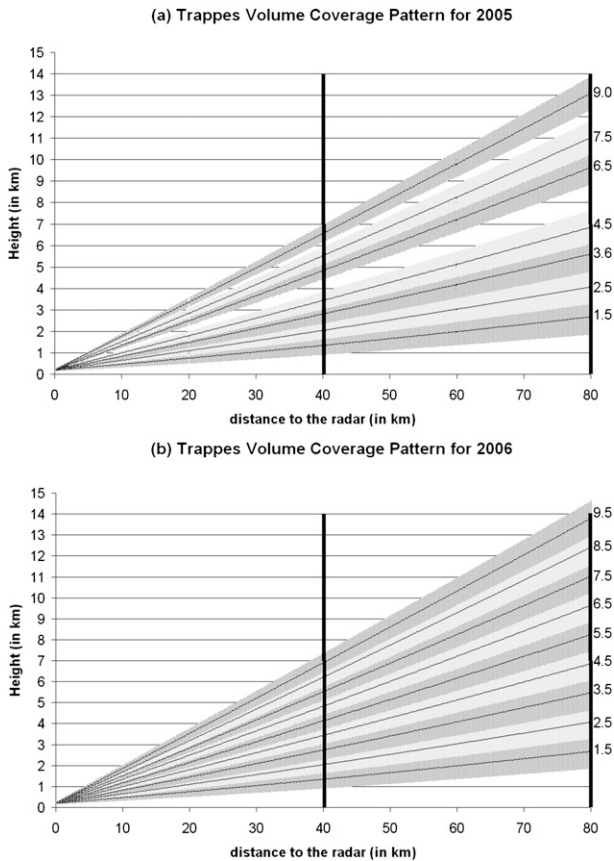


FIG. 2. Scan strategy of the Trappes radar in (a) 2005 and (b) 2006. The vertical bars at 40 and 80 km indicate the area where the retrieval of the vertical profile can be done.

sufficient while mesoscale model forecasts of the wet-bulb temperature fields may not be relevant for the inner part of the convective cells, where significant latent heat release is expected. Jameson (1992) has suggested that the  $\gamma_H$  and  $\gamma_{DP}$  parameters are typically multiplied by a factor of 1.5 when the temperature decreases from 20° down to 0°C.

In addition to characterizing the attenuating cells in terms of  $Z_H$ ,  $Z_{DR}$ , temperature,  $K_{DP}$ , and  $\rho_{HV}$ , we also considered the vertical profile of reflectivity in the most intense part of the attenuating cells, as this is widely used to indicate the presence of hail at ground level. Several indicators [ $Z_H > 55$  dBZ, vertically integrated liquid content, probability of hail (POH), etc.] have been proposed and validated to identify the presence of hail within convective cells (Waldvogel et al. 1979; Eilts et al. 1996; Witt et al. 1998; Joe et al. 2004; Delobbe and Holleman 2006). While it is recognized that those conventional methods typically do not attempt to estimate the height or the size of the hailstones, they have proven to be efficient enough to be used by many

operational services to diagnose the presence of hail at ground level. As will be seen later, a central question for the present work and more generally for all attenuation correction methods at C band (Ryzhkov et al. 2007) is whether the attenuating cells contain hail, a rain/hail mixture, or pure rain.

The scan strategy for the Trappes radar for the years 2005 and 2006 is presented in Fig. 2. The elevation angles are scanned on a 15-min basis and range from 1.5° to 9° (9.5° for the year 2006). Two additional low-elevation angles (0.4° and 0.8°) are actually revisited every 5 min, but they were considered to be too much affected by beam blockage and radome interferences for use in the present analysis. Because of this limited number of elevation angles, the vertical structure could only be recovered for ranges between 40 and 80 km. To reconstruct the vertical profile, horizontal reflectivity data were synchronized using a standard cross-correlation advection field at the end of the 15-min period and corrected for attenuation using filtered  $\Phi_{DP}$  and the appropriate  $\gamma_H$  (i.e., the one retrieved following the approach described previously). The vertical profile was then extracted at the range of maximum  $Z_H$ .

### b. Examples

Figure 3 shows an example of the application of the method on a particular ray. Data were taken at 1.5° during a convective situation (1630 UTC 23 June 2005). The raw  $Z_H$  and  $Z_{DR}$  profiles are represented by thin lines and their attenuation-corrected counterparts by thick lines. Profiles of raw  $\phi_{DP}$  (noisy thin line), seven-gate, median-filtered  $\phi_{DP}$  (thick line),  $K_{DP}$ , and  $\rho_{HV}$  are also plotted in Fig. 3 and show that the total differential phase shift is more than 100°. The PIA and PIDA are in this case respectively equal to 10 and 3 dB, and  $\gamma_{DP}$  was estimated at 0.025 dB °<sup>-1</sup>, a typical value (Carey et al. 2000; G06; Ryzhkov et al. 2007). In the most intense part of the attenuating cell (in terms of  $Z_H$ , see the vertical bar),  $Z_H$  reaches 51.5 dBZ,  $Z_{DR}$  reaches 2.78 dB, and  $K_{DP}$  reaches 3.9° km<sup>-1</sup>. It is noteworthy that  $\rho_{HV}$  decreases down to 0.93;  $\rho_{HV}$  normally decreases in convective cells when hydrometeors with a large variety of shapes are present. This occurs in heavy rain when large and small drops are both present (e.g., Keenan et al. 2001, their Fig. 10) and when there are rain/hail mixtures, particularly when the hail is large enough to Mie scatter. In addition, low values of  $\rho_{HV}$  can occur when there are high gradients of reflectivity within the resolution volume (e.g., Ryzhkov 2007). The vertical reflectivity profile steadily decreases from 53 dBZ at the lower levels to 33 dBZ at 10 km. The 45-dBZ level is reached approximately at the height ( $H_{45dBZ}$ ) of 7 km.

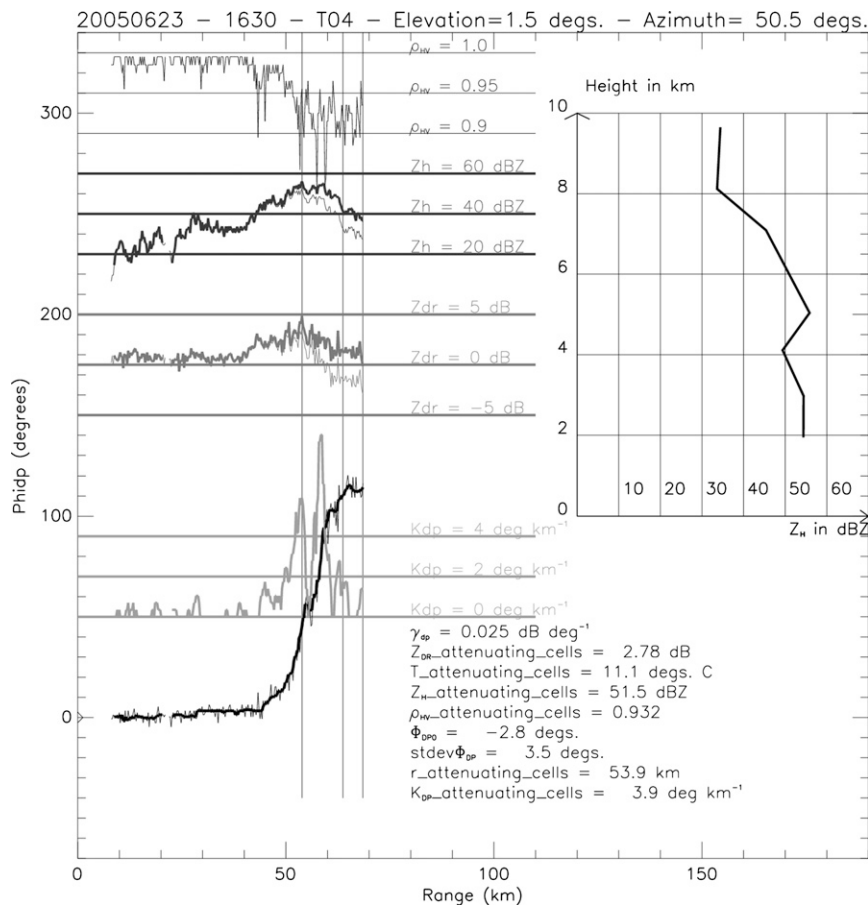


FIG. 3. Range profiles of raw and filtered  $\Phi_{DP}$ ,  $K_{DP}$ , raw and corrected  $Z_{DR}$  and  $Z_H$ , and  $\rho_{HV}$ . Those profiles have been obtained at the elevation of  $1.5^\circ$  at 1630 UTC 23 Jun 2005. The values of the  $\gamma_{DP}$  parameter and the properties of the attenuating cells ( $Z_{DR}$ , temperature,  $Z_H$ ,  $\rho_{HV}$ ) are given. All profiles have been corrected for nonprecipitation echoes.  $Z_H$  and  $Z_{DR}$  were corrected for attenuation using the procedure described in section 2. The  $\Phi_{DP}$  profile has been corrected for the system differential phase, the value of which— $\Phi_{DP0}$ —is given on the graph. Two  $\phi_{DP}$  profiles are presented on the graph: the raw profile (thin noisy line) and the median-filtered profile (thick smooth curve). Also indicated are the std dev of  $\Phi_{DP}$  ( $stdev\Phi_{DP}$ ) in the stratiform region and the range of the maximum of  $K_{DP}$  ( $r_{attenuating\_cells}$ ). The vertical profile of (horizontal) reflectivity was retrieved from the set of PPIs of the volume scan.

The  $0^\circ\text{C}$  isotherm height ( $H_{0^\circ\text{Cisotherm}}$ ) for that day was at 3.5 km above sea level. Using Delobbe and Holleman's (2006) formula to assess the probability of hail (POH),

$$\text{POH} = 0.319 + 0.133(H_{45\text{dBZ}} - H_{0^\circ\text{Cisotherm}}), \quad (18)$$

we get a POH of 0.78. Even though (18) has not been tuned specifically for the Trappes region, one can say that there is presumption of hail in that cell. We recall here that comparisons with surface reports have shown that the conventional POH estimator is fairly successful at predicting hail at ground level. Since in this work we are mainly using data from low-elevation angles at short distances from the radar (i.e., close to the ground),

it is fair to assess the presence of hail in the plan position indicator (PPI) using the conventional POH estimator.

Figure 4 is taken from the same episode as Fig. 3 (23 June 2005) but at a slightly different time (1600 UTC) and in another azimuth. The amount of total differential phase shift is about the same as in Fig. 3 (a little more than  $100^\circ$ ). Yet in that case, the attenuation is much more severe; the PIA and PIDA values are respectively equal to 20 and 5 dB. The estimated  $\gamma_{DP}$  is equal to  $0.056 \text{ dB } ^\circ\text{ }^{-1}$  (i.e., more than twice as large as in the previous example). Figures 3 and 4 clearly illustrate the fact that the coefficient of proportionality between  $A_{DP}$  and  $K_{DP}$  in (2) does not depend solely upon temperature.

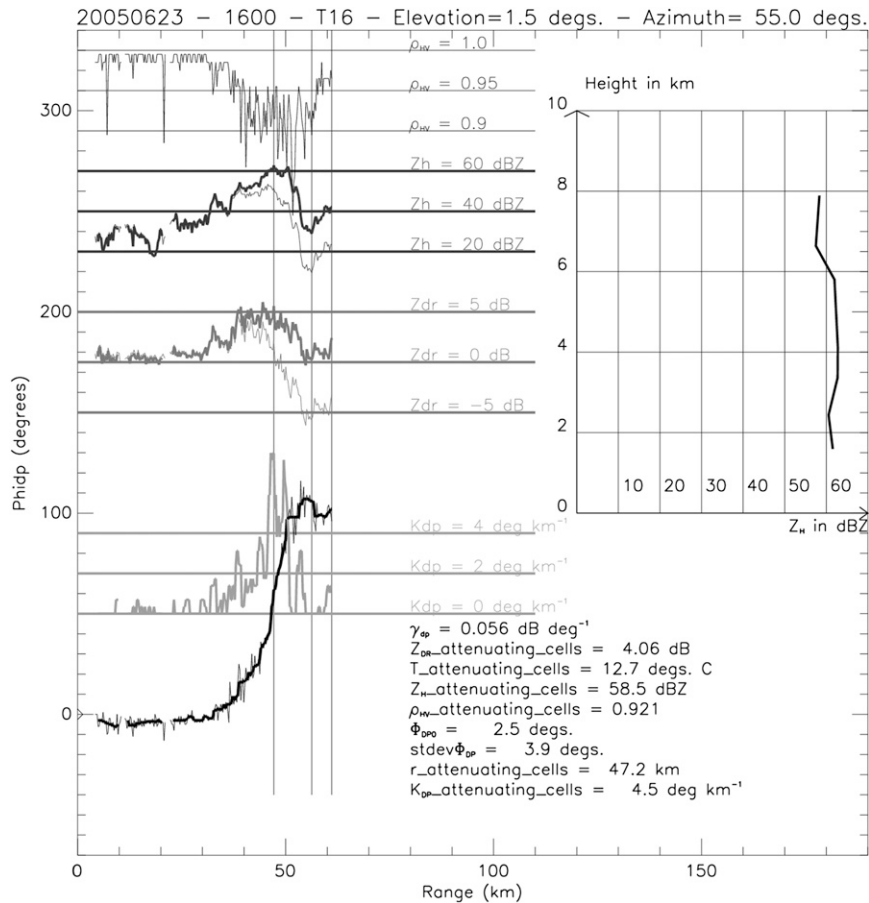


FIG. 4. As in Fig. 3 but at a slightly different time (1600 UTC) and in another azimuth.

The central question is then to know whether the attenuating cells have significantly different characteristics in the two cases. The  $\rho_{HV}$  pattern is rather similar in both cases. A careful examination though reveals a tendency in the second case (the one with high  $\gamma_{DP}$ ) to have slightly lower values of  $\rho_{HV}$ , with some spikes even below 0.9. Likewise, the  $K_{DP}$  profiles are comparable, though higher in the high  $\gamma_{DP}$  case, in terms of maximum ( $\sim 4^\circ \text{ km}^{-1}$ ) and range extension (20 km). On the other hand, there is a very sharp contrast between the  $Z_H$  and even more between the  $Z_{DR}$  profiles. In the high  $\gamma_{DP}$  case,  $Z_H$  reaches 58.5 dBZ and  $Z_{DR}$  4 dB over almost 10 km. The vertical profile of reflectivity is almost vertical and beyond 60 dBZ up to 6 km. Given the limited vertical coverage, the top of the cell cannot be determined with a high degree of accuracy but one can expect that the POH would probably be beyond 1.

Before moving on to the analysis of all the observations, Fig. 5 illustrates one limitation of the present approach. In this situation, two attenuating cells are clearly visible on the profile: the first one produces a differential phase shift of  $20^\circ$  (maximum  $Z_H$  of 50 dBZ)

and the other produces  $100^\circ$  (maximum  $Z_H$  of 58 dBZ). A stratiform region was identified between 50 and 55 km and the properties of the attenuating cells were automatically extracted using (13)–(16). Given the linear  $Z_H$  weighting used in the equations, basically only the second cell was considered when retrieving  $Z_H$ ,  $Z_{DR}$ , temperature,  $K_{DP}$ , and  $\rho_{HV}$ . A better approach would have consisted of splitting the ray into two parts, analyzing the first part, retrieving the appropriate  $\gamma_H$  and  $\gamma_{DP}$ , correcting  $Z_H$  and  $Z_{DR}$  for attenuation, and then processing the second part. This refinement has not been introduced mainly because a subjective overview of all the profiles showed that, in the vast majority of the cases, attenuation was due to a well-defined single attenuating cell.

### 3. Results

#### a. Introduction

The method proposed in the previous section has been applied to more than 30 convective and mixed cases observed during 2005 and 2006. All tilts between  $1.5^\circ$

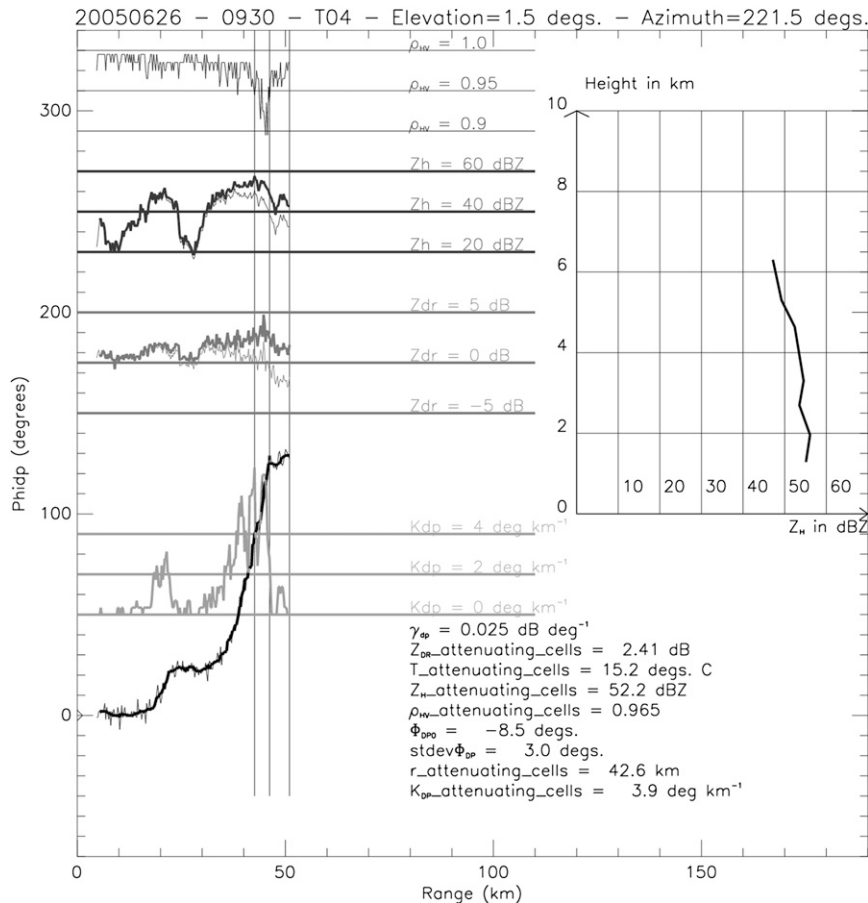


FIG. 5. As in Fig. 3 but for another episode (0930 UTC 26 Jun 2005).

and  $9^\circ$  were considered. The freezing-level height varies between 1 and 3.5 km above mean sea level (MSL), the radar being located at 191 m MSL. However, most of the attenuating cells correspond to summer events with freezing-level heights typically at 3 km MSL. For each suitable ray, the following parameters were computed and stored: PIA (dB), PIDA (dB),  $\gamma_{DP}$  ( $\text{dB } ^\circ^{-1}$ ),  $\gamma_H$  ( $\text{dB } ^\circ^{-1}$ ),  $T_{\text{attenuating\_cells}}$  ( $^\circ\text{C}$ ),  $Z_{DR}^{\text{attenuating\_cells}}$  (dB),  $Z_H^{\text{attenuating\_cells}}$  (dBZ),  $\rho_{HV}^{\text{attenuating\_cells}}$  (dimensionless),  $K_{DP}^{\text{attenuating\_cells}}$  ( $^\circ \text{ km}^{-1}$ ),  $r_{\text{attenuating\_cells}}$  (km), system differential phase ( $\Phi_{DP0}$ ), and standard deviation of the differential phase in the stratiform region ( $\text{std dev } \Phi_{DP}$ ). Overall, the dataset comprises 216 519 profiles. We have calculated that the S&I constraint could only be applied to 20% of all attenuated rays (defined by  $\Phi_{DP} > 30^\circ$ ). For 80% of the rays having a significant differential phase shift ( $\Phi_{DP} > 30^\circ$ ), no suitable stratiform region could be identified, either because a plateau of  $\Phi_{DP}$  could not be found in the rain region, the standard deviation of  $\Phi_{DP}$  was too high ( $>5^\circ$ ),  $Z_H$  was too high, or the SNR too low. This means that the S&I constraint does not qualify for

operational attenuation correction of dual-polarization measurements. Also stored in the database are the vertical profiles of horizontal reflectivity ( $Z_H$ ) for the attenuating cells located between 40 and 80 km. This information was only available for 10% of all the attenuating cells present in the database.

Figure 6 introduces the quantitative analysis. It simply represents the mean  $\pm 1/10$  (for visibility purposes) of the standard deviation of the PIDA (dB) as a function of the total differential phase shift ( $\Delta\Phi_{DP}$ ;  $^\circ$ ) for a narrow range of temperature ( $12.5^\circ < T < 17.5^\circ\text{C}$ ) and for different values of  $Z_{DR}^{\text{attenuating\_cells}}$  (i.e., the  $Z_{DR}$  value of the attenuating cells). All curves in Fig. 6 are approximately linear, which establishes the relevance of (2). Also noteworthy is the fact that their slopes (i.e., the  $\gamma_{DP}$  parameter) seem to be increasing with  $Z_{DR}^{\text{attenuating\_cells}}$ , consistent with previous works (Carey et al. 2000; Brangi and Chandrasekar 2001; G06). The subsequent analyses aim at precisely assessing the relationship between  $\gamma_{DP}$  and the polarimetric values of the attenuating cells.



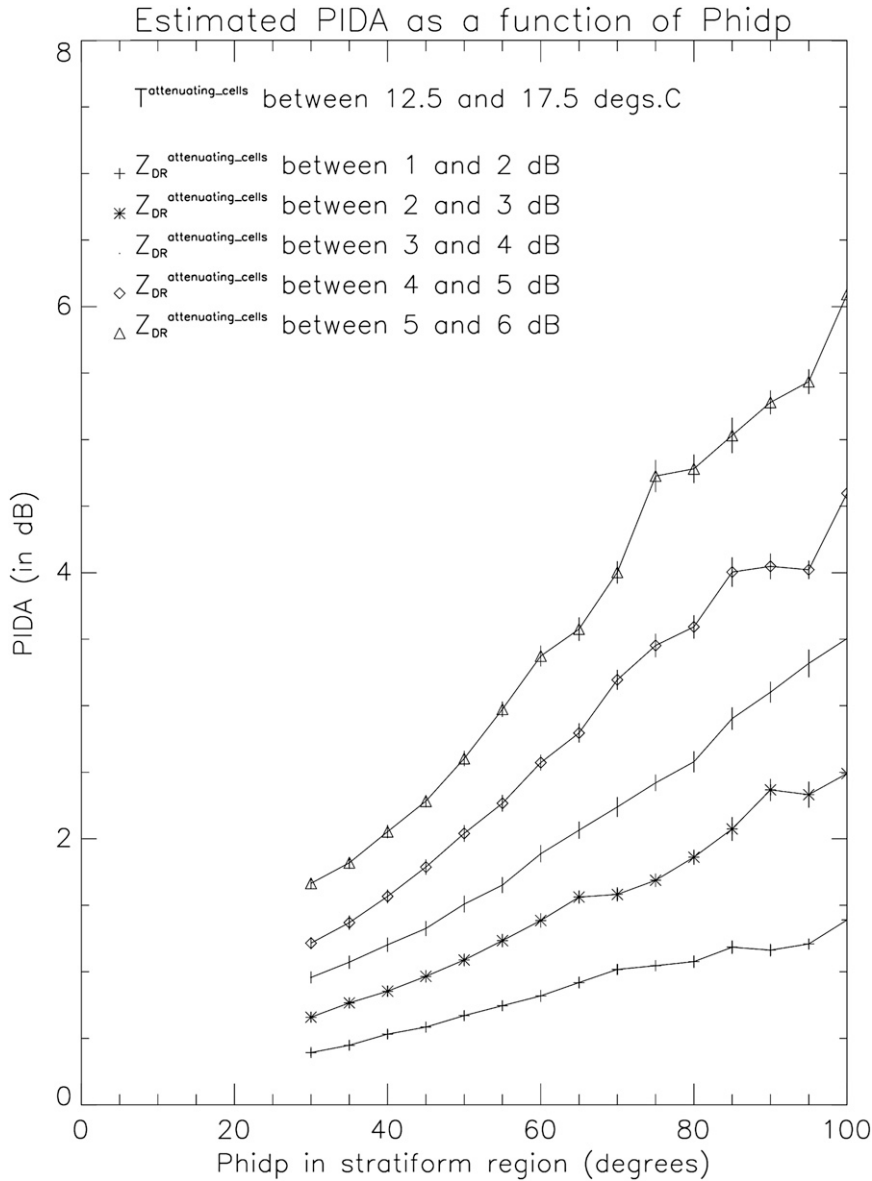


FIG. 6. PIDA (dB) as a function of the normalized differential phase ( $\phi_{DP}$ ,  $^{\circ}$ ) for different values of  $Z_{DR}^{\text{attenuating\_cells}}$  and for a fixed temperature ( $12.5^{\circ} < T < 17.5^{\circ}\text{C}$ ). Vertical bars correspond to  $\pm 1/10$  (for visibility purposes) of the std dev.

*b. Stratification of the observed attenuating cell properties with  $\gamma_{DP}$*

Figure 7 presents a stratification of the results according to the estimated  $\gamma_{DP}$ , with and without the coupling between  $\gamma_H$  and  $\gamma_{DP}$  being activated in the retrieval in (12). For clarity, no standard deviation bars are presented. We shall first comment on results obtained with the coupling activated. The basic idea of that first stratification is to characterize the properties of the attenuating cells leading to high  $\gamma_{DP}$  values. First of

all, Fig. 7a presents the overall and day-by-day occurrence frequency of the estimated  $\gamma_{DP}$ . The vertical scale is logarithmic. The maximum frequency is centered at  $0.025 \text{ dB } ^{\circ^{-1}}$ , which is a value that compares quite well to previously reported results. The distribution is rather broad and values beyond  $0.06 \text{ dB } ^{\circ^{-1}}$  occur for 15%—a nonnegligible figure—of the rays presenting a significant differential phase shift ( $>30^{\circ}$ ). Several episodes lead to such high  $\gamma_{DP}$  values. This is a convincing demonstration that the variability of the  $\gamma_{DP}$  coefficient has to be accounted for in any operational

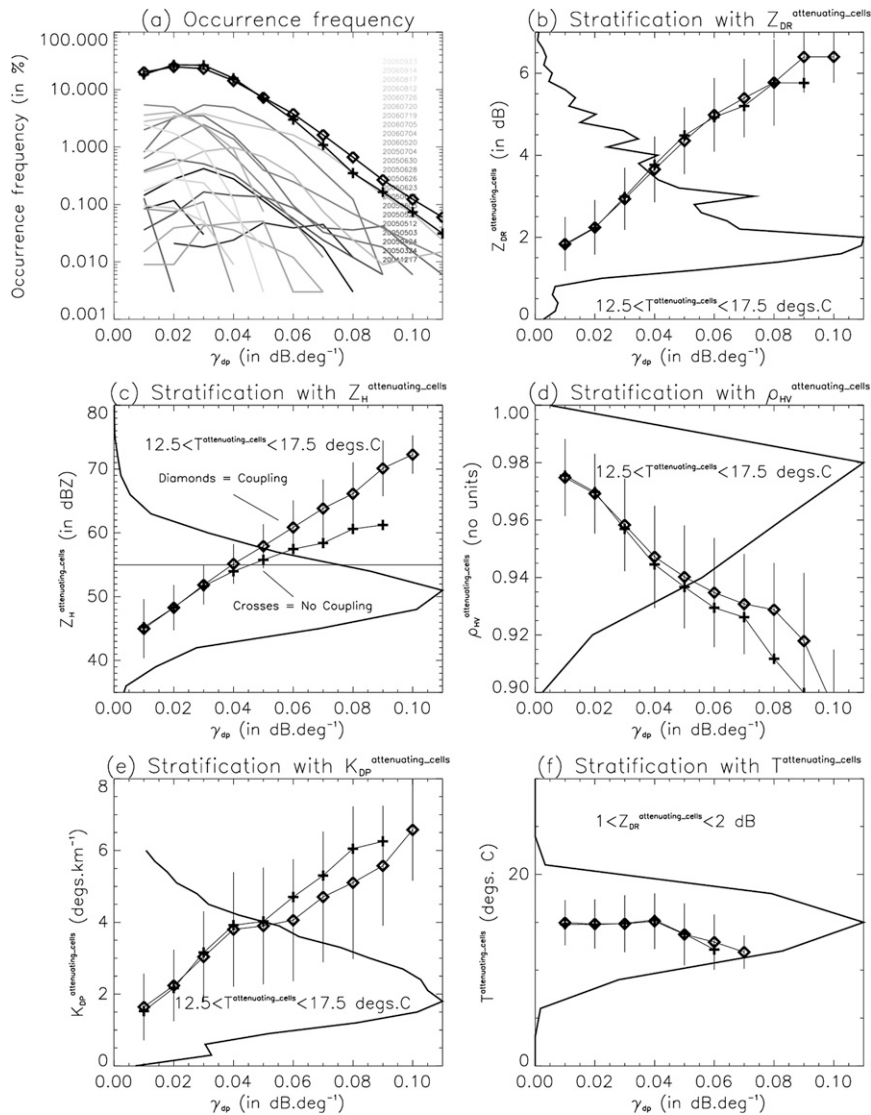


FIG. 7. Overall and day-by-day occurrence frequency of (a)  $\gamma_{DP}$  and characteristics of the attenuating cells in terms of (b)  $Z_{DR}$ , (c)  $Z_H$ , (d)  $\rho_{HV}$ , (e)  $K_{DP}$ , and (f)  $T$  as functions of the S&I retrieved  $\gamma_{DP}$ . Panels (b)–(e) can be considered as stratifications at a fixed temperature ( $15^\circ\text{C}$ ) while (f) is a stratification at fixed  $Z_{DR}$  ( $Z_{DR} = 1.5 \text{ dB}$ ). The bin size for  $\gamma_{DP}$  is  $0.01 \text{ dB} \cdot \text{deg}^{-1}$ . For each parameter, the mean (diamond)  $\pm$  std dev is plotted. Also shown in (b)–(f) are the histograms of the attenuating cell characteristics. Results without the coupling activated correspond to crosses.

attenuation correction procedure. More recently, Ryzhkov et al. (2007), using independent data from the two SIDPOL C-band polarimetric radars in Alabama and in Canada and a rather different methodology to estimate  $\gamma_{DP}$ , also found a large variability of  $\gamma_{DP}$  (see their Table 1). The typical median values they obtained for Alabama were  $0.01$  (tropical rain),  $0.02$  (rain with hail), and  $0.01$  (tornado)  $\text{dB} \cdot \text{deg}^{-1}$ . In Canada, the typical median values of  $\gamma_{DP}$  were  $0.01$ – $0.04$  (small hail),  $0.01$  (rain),  $0.08$  (hail), and  $0.03$ – $0.06$  (rain with hail)  $\text{dB} \cdot \text{deg}^{-1}$ .

Figures 7b–e show respectively the mean  $Z_{DR}$ ,  $Z_H$ ,  $\rho_{HV}$ , and  $K_{DP}$  values of the attenuating cells as a function of  $\gamma_{DP}$ . To avoid confusion and competing effects between temperature and DSD characteristics and shapes, these plots are for data all having similar temperatures ( $T^{\text{attenuating\_cells}}$  between  $12.5^\circ$  and  $17.5^\circ\text{C}$ ). Therefore, one can say that temperature plays a negligible role in the trends observed in Figs. 7b–e. There is a clear linear relationship between  $\gamma_{DP}$  and each of the four above-mentioned variables ( $Z_{DR}^{\text{attenuating\_cells}}$ ,

$Z_H^{\text{attenuating\_cells}}$ ,  $\rho_{\text{HV}}^{\text{attenuating\_cells}}$ , and  $K_{\text{DP}}^{\text{attenuating\_cells}}$ ). Larger  $\gamma_{\text{DP}}$  values statistically correspond to larger  $Z_{\text{DR}}$ , larger  $Z_H$ , smaller  $\rho_{\text{HV}}$ , and larger  $K_{\text{DP}}$ . In particular, the unusually high  $\gamma_{\text{DP}}$  values (say beyond  $0.06 \text{ dB } ^\circ^{-1}$ ) that we will show are very unlikely in rain are caused by cells with  $Z_{\text{DR}}$  beyond 5 dB,  $Z_H$  beyond 60 dBZ,  $\rho_{\text{HV}}$  below 0.94, and  $K_{\text{DP}}$  above  $4^\circ \text{ km}^{-1}$ . Those cells are likely to contain frozen particles (hail or graupel) mixed with rain since such low values of  $\rho_{\text{HV}}$  are unlikely in rain.

Interestingly, the “high”  $\gamma_{\text{DP}}$  regime (above  $0.06 \text{ dB } ^\circ^{-1}$ ) seems simply to be the linear extrapolation of the “low” regime (below  $0.06 \text{ dB } ^\circ^{-1}$ ). Among all the storms that were included in the database, some are known to have been hail producing (Vulpiani et al. 2008). The presence of ice leads to an expected increase in values of  $Z_H$ , but also more surprisingly, increases in  $Z_{\text{DR}}$  and  $K_{\text{DP}}$ . This seriously questions the usability of  $K_{\text{DP}}$  to retrieve rain rate in the presence of ice. Finally, Fig. 7f presents the relationship between  $T^{\text{attenuating\_cells}}$  and  $\gamma_{\text{DP}}$ . Similarly to what was done to remove any temperature impact on Figs. 7b–e, Fig. 7f was built from data having all the same  $Z_{\text{DR}}$  ( $Z_{\text{DR}}^{\text{attenuating\_cells}}$  between 1 and 2 dB). Figure 7f does not reveal any clear relationship between  $\gamma_{\text{DP}}$  and  $T^{\text{attenuating\_cells}}$ . This may be explained by the fact that the range of  $T^{\text{attenuating\_cells}}$  present in the database is rather modest (say between  $10^\circ$  and  $20^\circ\text{C}$ ). Climatologically speaking, the majority of attenuating precipitation systems occur in France at the same season in about the same temperature conditions ( $15^\circ\text{C}$ ). Operational attenuation correction algorithms should try to take into account the temperature effect but it is clearly second order compared with the impact of the microphysical characteristics of the attenuating cells.

The presence of ice in the attenuating cells calls into question the application of a coupling between  $\gamma_H$  and  $\gamma_{\text{DP}}$ . Indeed, the 0.3 factor between  $\gamma_H$  and  $\gamma_{\text{DP}}$  was established using scattering simulations and disdrometer observations in pure rain and little is known about the evolution of the proportionality factor in the presence of ice. This is the reason why a “no coupling” analysis has been carried out where  $\gamma_H$  is set to a climatological value ( $0.1 \text{ dB } ^\circ^{-1}$ ). Results of this experiment are indicated by crosses on Fig. 7. As expected, the variable that is mostly affected is  $Z_H^{\text{attenuating\_cells}}$ . In the “coupling” experiment, it reaches the unrealistic value of 72 dBZ (for  $\gamma_{\text{DP}}$  equal  $0.1 \text{ dB } ^\circ^{-1}$ ) while in the no coupling experiment, it peaks at 60 dBZ, still an extremely high value that would be consistent with the presence of wet ice. Because it is very likely that unusually high  $\gamma_{\text{DP}}$  leads to unusually high  $\gamma_H$  (in a proportion that is unknown), it is fair to admit that the no coupling curve stands as the minimum bound of  $Z_H^{\text{attenuating\_cells}}$  while the coupling curve can be consid-

ered as its maximum bound. The  $Z_{\text{DR}}^{\text{attenuating\_cells}}$  curve (Fig. 7b) changes a little bit toward slightly lower values for extremely high  $\gamma_{\text{DP}}$ , which is the logical consequence of lower  $\gamma_H$ , hence lower  $Z_H$  and  $Z_{\text{DR}}$  values in the stratiform region and lower estimated  $\gamma_{\text{DP}}$ . The  $\rho_{\text{HV}}^{\text{attenuating\_cells}}$  (Fig. 7d) and  $K_{\text{DP}}^{\text{attenuating\_cells}}$  (Fig. 7e) are also slightly altered because of the change of the attenuation-corrected  $Z_H$  values that are used as weights in the extraction of the properties of the attenuating cells [(13)–(17)]. Overall, the coupling and no coupling curves can be regarded as uncertainty bounds attached to the estimated polarimetric variables of the attenuating cells. The conclusions regarding the surprisingly very high values of  $\gamma_{\text{DP}}$ ,  $K_{\text{DP}}$ , and  $Z_{\text{DR}}$  and the likelihood of (wet) ice remain whether the coupling is considered or not.

### c. Comparison with simulations based on Chilbolton disdrometer data

Figure 8 is another way to look statistically at the results. The stratification of the radar observations is done this time according to the properties of the attenuating cells ( $Z_{\text{DR}}^{\text{attenuating\_cells}}$ ,  $Z_H^{\text{attenuating\_cells}}$ ,  $\rho_{\text{HV}}^{\text{attenuating\_cells}}$ ,  $K_{\text{DP}}^{\text{attenuating\_cells}}$ ) and for various temperature ranges. In addition, on the left-hand side of Fig. 8, we present computations of these variables using raindrop size spectra obtained with a Joss–Waldogel disdrometer over the period June 2003–June 2008 (i.e., 4 yr) sited at Chilbolton (Hampshire, United Kingdom). Chilbolton is located less than 400 km northwest of Trappes. Chilbolton is the closest site to Trappes where long time series of reliable disdrometer data are available. Both sites have a maritime climate with similar total annual rainfall distributed throughout the year but with a very slight tendency to more convective precipitation at Trappes. Table 1 gives the seasonal statistics of rainfall accumulations computed over the period 1971–2000 for Paris and London. It is thus fair to assume that the rain systems affecting both sites have, on average, similar microphysical properties. Because we are interested in events with unusually high attenuation, extreme care is needed to ensure that the disdrometer is operating reliably during the heaviest rain, which occurs only for brief periods. Analysis of the data reveals occasional very short periods of apparently heavy rain composed of only very large drops; closer examination of other gauges showed no rain was falling and that the large drops were probably spurious and caused by crows attacking the Styrofoam cover of the disdrometer. To remove such spurious data, the disdrometer data were compared with three gauges each recording the individual drops (equivalent to 0.004 mm of rain) forming at the base of the gauge funnel; each 30-s disdrometer spectrum was only accepted when two of the three drop

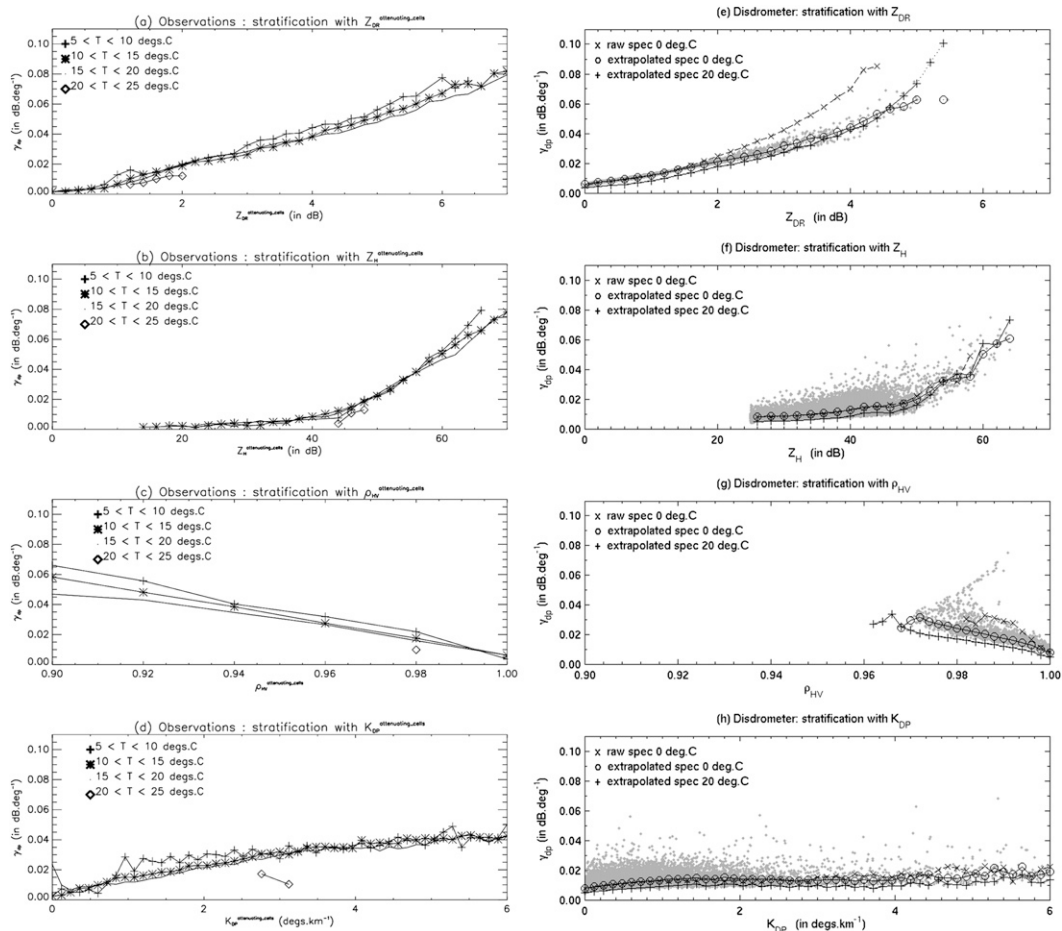


FIG. 8. The  $\gamma_{DP}$  as a function of (a),(e)  $Z_{DR}^{\text{attenuating\_cells}}$ , (b),(f)  $Z_H^{\text{attenuating\_cells}}$ , (c),(g)  $\rho_{HV}^{\text{attenuating\_cells}}$ , and (d),(h)  $K_{DP}^{\text{attenuating\_cells}}$ . Panels (a)–(d) correspond to observations and panels (e)–(h) correspond to simulations based on Chilbolton observed spectra. Different temperature ranges are analyzed.

counting gauges recorded some rainfall. The disdrometer calibration was monitored by comparing weekly rainfall totals with those from a conventional gauge and any periods of questionable calibration were rejected. After this rigorous quality control, a total of 109 551 spectra were accepted.

The next stage of the disdrometer analysis is to compute values of  $Z_H$ ,  $Z_{DR}$ ,  $K_{DP}$ ,  $\rho_{HV}$ ,  $\gamma_H$ , and  $\gamma_{DP}$  at  $0^\circ\text{C}$  using the **T**-matrix solution technique (Mishchenko 2000) to account for any Mie scattering and resonance at C band and the raindrop axis ratio relationship proposed by Brandes et al. (2002), which has been confirmed as appropriate for rain observed in northern France (Gourley et al. 2009). The 52 500 spectra with a  $Z_H$  above 25 dBZ (rain rates above about  $1 \text{ mm h}^{-1}$ ) were selected and the values of  $Z_{DR}$ ,  $Z_H$ ,  $\rho_{HV}$ , and  $K_{DP}$  plotted as a function of  $\gamma_{DP}$  in Figs. 8e–h, respectively, where the individual points are in gray and the mean values are crosses. Analysis for values of  $Z_H$  above

45 dBZ (not shown) showed a linear relationship between  $\gamma_H$  and  $\gamma_{DP}$  with a very high correlation and a slope of 0.3, thus justifying our fundamental assumption in (12).

In the heaviest rain, the upper limit of 5 mm for the disdrometer may be truncating the spectra and eliminating the largest drops, which may be contributing significantly to the attenuation and the polarization parameters. To account for the truncation, we consider the

TABLE 1. The 1971–2000 rainfall amount statistics in Paris and London.

Mean rainfall amount	Paris	London
January–March	145.9	127.9
April–June	172.6	145.4
July–September	160.9	142.5
October–December	170.3	167.8
Total	649.7	583.6

counts in the last bin (bin no. 127), which provides the total number of drops above 5 mm. Because of saturation of the instrument, drops with a diameter beyond that threshold cannot be accurately sized. The last bin count was nonzero for 201 spectra and reached 23 in the heaviest rainfall cases. To extrapolate the spectra to include the larger drops we fitted our observed truncated spectra to a normalized gamma function of the form  $N(D) = N_W(D/D_0)^\mu \exp[-(3.67 + \mu)D/D_0]$  using the method of moments as described by Kozi and Nakamura (1991). The fitted values obtained are very reasonable. The mean value of  $\log(N_W)$  is  $3.8 \text{ mm}^{-1} \text{ m}^{-3}$  with a standard deviation of 5 dB,  $D_0$  peaks at 1.1 mm with a tail extending to 4 mm, and the  $\mu$  distribution is quite skewed with a median of 5 and a long tail of positive values. To recreate the missing large drops the full untruncated spectrum was computed from the fits, and the number of drops  $>5$  mm that the disdrometer would have classified in its last bin (bin no.127) was calculated. A scatterplot of the number of predicted drops above 5 mm with those observed was very encouraging. For 218 spectra the extrapolated fit predicted one or more drops  $>5$  mm, and the maximum number of predicted large drops  $>5$  mm was 22. On average the extrapolated predicted count was within 3 counts of the observed number.

The values of  $Z_H$ ,  $Z_{DR}$ ,  $\rho_{HV}$ ,  $K_{DP}$ ,  $A_H$ , and  $A_{DP}$  were computed from the 52 500 spectra fitted to a gamma function and the mean values of  $Z_{DR}$ ,  $Z_H$ ,  $\rho_{HV}$ , and  $K_{DP}$  plotted in Figs. 8e–h as a function of  $\gamma_{DP}$  for  $0^\circ$  and  $20^\circ\text{C}$ . The impact of the extrapolated large drops is, as expected, really only significant for  $Z_{DR}$ , where for  $Z_{DR} > 3$  dB the inclusion of the extrapolated large drops increases  $Z_{DR}$  by about 1 dB. This change does, however, lead to a much better agreement with the radar observations in Fig. 8a. Note also that the computations using the disdrometer spectra predict a very slight increase in attenuation at the lower temperature, also in agreement with the radar observations. A maximum size of 10 mm was assumed for the extrapolated spectra in Fig. 8, but reducing this to 8 mm did not change the plots significantly; most of the fitted spectra had a positive  $\mu$ , which introduces a natural truncation of the spectrum. The plot of  $Z_{DR}$  against  $\gamma_{DP}$  at  $20^\circ\text{C}$  for  $Z_{DR} > 5$  dB is shown dotted in Fig. 8e because there are only three data points. We note that the highest value of  $\gamma_{DP}$  in nearly all naturally occurring rainfall is  $0.06 \text{ dB } ^\circ^{-1}$  and the minimum value of  $\rho_{HV}$  derived from the spectra is 0.96, which may be reduced by radar imperfections to 0.95. In their analysis of a large dataset of tropical raindrop spectra, Keenan et al. (2001) found a similar minimum (their Fig. 10). In their Fig. 9, the vast majority of spectra had a  $\gamma_{DP}$  below  $0.06 \text{ dB } ^\circ^{-1}$ , with just a very few tropical

spectra above this value when a maximum drop size of  $2.5 D_0$  was assumed but not for an 8-mm maximum drop size. This suggests that values of  $\rho_{HV}$  lower than 0.95 and  $\gamma_{DP}$  above  $0.06 \text{ dB } ^\circ^{-1}$  found in hot spots in northwest Europe are only rarely due to pure rain but usually indicate targets that include some wet ice.

We now consider the implications of Fig. 8. Figure 8a (mean  $\gamma_{DP}$  value as a function of  $Z_{DR}^{\text{attenuating\_cells}}$ ) shows that  $Z_{DR}^{\text{attenuating\_cells}}$  is an excellent predictor of the  $\gamma_{DP}$  value. The corresponding disdrometer calculations (Fig. 8e) reproduce the  $Z_{DR}$  dependency very well but only up to 5 dB and  $\gamma_{DP}$  of  $0.06 \text{ dB } ^\circ^{-1}$  indicating that values above these limits are likely to be due to partially frozen particles.

Figures 8b and 8f reveal an excellent agreement between the observed and simulated  $\gamma_{DP} = f(Z_H^{\text{attenuating\_cells}})$  relationships, with both predicting, for example, values of  $\gamma_{DP}$  of 0.02 and  $0.04 \text{ dB } ^\circ^{-1}$ , for a mean  $Z_H$  of 50 and 60 dBZ, respectively. There again, however, the disdrometer predicts no values of  $\gamma_{DP}$  above  $0.06 \text{ dB } ^\circ^{-1}$ . Figures 8c and 8g show  $\rho_{HV}$  plotted as a function of  $\gamma_{DP}$ . Lower values of  $\rho_{HV}$  are clearly associated with higher values of  $\gamma_{DP}$  both on the observations and on the simulations. However, simulations do not yield  $\rho_{HV}$  values below 0.96 (corresponding to  $\gamma_{DP}$  equal to  $0.04 \text{ dB } ^\circ^{-1}$ ). This can be interpreted as further evidence that the attenuating hydrometeors are most unlikely to be pure rain in the “low  $\rho_{HV}$ –high  $\gamma_{DP}$ ” regime. We note that the melting model of hail presented by Rasmussen and Heymsfield (1987), whereby a torus of water forms around the equator of a melting hailstone leading to a stable nontumbling fall mode, is consistent with the “hot spots” having very high  $Z_H$  and  $Z_{DR}$ , low  $\rho_{HV}$ , and very large total and differential attenuation. Finally, observed and simulated  $\gamma_{DP} = f(K_{DP}^{\text{attenuating\_cells}})$  curves (Figs. 8d,h) both show the same increasing trend, but the disdrometer curves are rather flatter with  $K_{DP}$  values approximately halved. The radar observations tend to show a much clearer increase of  $\gamma_{DP}$  with increasing  $K_{DP}^{\text{attenuating\_cells}}$ , consistent with Fig. 7e. We recall here that observed  $K_{DP}$  have been estimated using a very short path (1.68 km) and should therefore be very close to intrinsic  $K_{DP}$ . The disagreement between observations and simulations can be interpreted as further evidence that ice is contributing to the high values of  $K_{DP}$  and to the attenuation in the hot spots.

#### d. Vertical profile analysis

To better assess the potential presence of frozen particles in the cells causing unusually high  $\gamma_{DP}$ , an analysis of the vertical profiles of horizontal reflectivity has been carried out. Figure 9 presents an analysis of

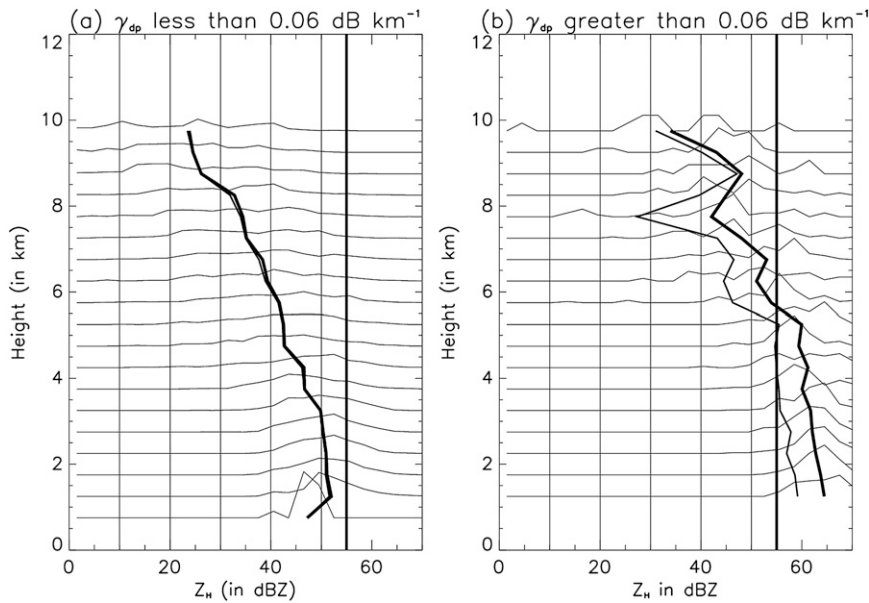


FIG. 9. Mean vertical profiles of reflectivity ( $Z_H$ ) in two contrasted cases: (a)  $\gamma_{DP} < 0.06 \text{ dB } \text{km}^{-1}$  and (b)  $\gamma_{DP} > 0.06 \text{ dB } \text{km}^{-1}$ . The histogram of  $Z_H$  for each height level between 1 and 10 km MSL is plotted. The vertical thick line corresponds to  $Z_H = 55 \text{ dBZ}$ .

those vertical profiles in two contrasting cases:  $\gamma_{DP} < 0.06 \text{ dB } \text{km}^{-1}$  (Fig. 9a) and  $\gamma_{DP} > 0.06 \text{ dB } \text{km}^{-1}$  (Fig. 9b). Two profiles are presented on each graph: the one retrieved with coupling between  $\gamma_H$  and  $\gamma_{DP}$  (thick line) and the one retrieved without coupling (thin line). In Fig. 9a, the coupling and the no coupling curves overlap completely and are hardly discernible. In Fig. 9b, the no coupling profile is about 5 dB smaller than the coupling profile. In all cases, the mean  $Z_H$  profiles are typical of convective cells. The profiles are almost vertical in the lowest layers (say up to 4 km), then decrease at the rate of  $-1.5 \text{ dB } \text{km}^{-1}$ . The high  $\gamma_{DP}$  profile, however, is shifted by about 5(10) dB in the no coupling (coupling) case toward higher  $Z_H$  than the low  $\gamma_{DP}$  profile. The low  $\gamma_{DP}$  profile is less than 55 dBZ at all heights whereas the high  $\gamma_{DP}$  profile exceeds that typical hail threshold up to 4(6) km MSL in the no coupling (coupling) case. The 45-dBZ contour is reached at about 4 km in the low  $\gamma_{DP}$  case and at some height above 7 km in the high  $\gamma_{DP}$  cases (with and without coupling). Assuming a  $0^\circ\text{C}$  isotherm height at 3 km, Eq. (18) gives values of POH of 0.45 (low  $\gamma_{DP}$  case) and a value above 0.85 (high  $\gamma_{DP}$  cases). This strongly supports that hail, possibly combined with rain, is present in the high  $\gamma_{DP}$  case.

#### 4. Conclusions

This paper has documented the variability of the coefficient  $\gamma_{DP}$  between the specific attenuation ( $A_{DP}$ ) and the

specific differential phase ( $K_{DP}$ ) retrieved from a 2-yr, C-band polarimetric dataset through the application of a physical constraint referred to as the ‘‘Smyth-and-Illingworth (S&I) constraint.’’ This constraint consists at first order in assuming that the intrinsic  $Z_{DR}$  in the low-reflectivity stratiform region behind convective cells is approximately equal to 0 dB. An empirical  $Z_{DR} = f(Z_H)$  distribution was built using a large number of non-attenuated, close-range, and high-SNR data and showed excellent agreement with the linear model proposed by Bringi et al. (2001). The empirical  $Z_{DR} = f(Z_H)$  relationship and a first guess of the attenuation-corrected  $Z_H$  were used to improve the estimation of  $Z_{DR}$  in the stratiform region. The S&I constraint has been implemented with and without a coupling between  $\gamma_H$  and  $\gamma_{DP}$ .

A thorough analysis of radar observations in Trappes (Gourley et al. 2009) indicated that the Brandes et al. (2002) raindrop shapes are appropriate with no evidence of oscillations in the heavier rain leading to unusual shapes; the self-consistency of the polarization parameters indicated that the raindrop spectra were well represented by normalized gamma functions—a conclusion confirmed by the analysis of four years of spectra in southern England. Accordingly, we are reasonably confident that in this study in northwest Europe a large majority of the highly attenuating ‘‘hot spots’’ that are accompanied by low  $\rho_{HV}$  do not result from raindrops alone. From the extensive analysis, which can very easily be reproduced for any other

polarimetric radar dataset, the following conclusions can be drawn:

- The S&I constraint, implemented as described above, could only be applied to 20% of all attenuated rays (defined by  $\Delta\Phi_{\text{DP}} > 30^\circ$ ). This means that operational differential attenuation correction algorithms cannot exclusively rely on the S&I constraint and that other correction techniques have to be used as an alternative. Any operational differential attenuation correction scheme should include a basic check on the sign of the corrected  $Z_{\text{DR}}$  values because no negative values are expected in rain.
- The range of variation of  $\gamma_{\text{DP}}$  is large and has to be accounted for in any operational algorithm. The minimum, maximum, and mean values are respectively equal to 0.01, 0.11, and  $0.025 \text{ dB } ^\circ\text{ }^{-1}$ . This is fully consistent with independent results obtained by Ryzhkov et al. (2007) in Alabama and Canada with the two SIDPOL radars.
- Another lesson of this work is that the impact of temperature on attenuation (hence on attenuation correction schemes) is clearly negligible compared to the impact of microphysical properties of the *attenuating cells*, as revealed by the values of the polarimetric variables. In addition to that, the majority of attenuating cells of the Paris area develop at the same season in the same thermal environment ( $T = 15^\circ\text{C}$ ).
- Surprisingly,  $\gamma_{\text{DP}}$  appears to be remarkably correlated (linearly) across its entire range of variation [ $0.01; 0.11$ ]  $\text{dB } ^\circ\text{ }^{-1}$  with the values of the polarimetric variables of the attenuating cells:  $Z_{\text{DR}}$ ,  $Z_{\text{H}}$ , and  $K_{\text{DP}}$  (positive correlation) and  $\rho_{\text{HV}}$  (negative correlation).
- For the sake of simplification, we have distinguished in the paper two  $\gamma_{\text{DP}}$  regimes: high  $\gamma_{\text{DP}}$  regime ( $>0.06 \text{ dB } ^\circ\text{ }^{-1}$ ) and low  $\gamma_{\text{DP}}$  regime ( $<0.06 \text{ dB } ^\circ\text{ }^{-1}$ ). Extremely high  $\gamma_{\text{DP}}$  values ( $>0.06 \text{ dB } ^\circ\text{ }^{-1}$ ) occur for 15%—a nonnegligible figure—of the rays presenting a significant differential phase shift ( $>30^\circ$ ). Those extremely high  $\gamma_{\text{DP}}$  values are caused by attenuating cells having unusually high (intrinsic)  $Z_{\text{DR}} > 4 \text{ dB}$ ,  $Z_{\text{H}} > 55 \text{ dB}$ , and  $K_{\text{DP}} > 4^\circ \text{ km}^{-1}$ , and unusually low  $\rho_{\text{HV}} < 0.94$ . This low  $\rho_{\text{HV}}$  regime is only very rarely reproduced by scattering simulations in pure rain using normalized gamma drop size distributions or by computations based on observed raindrop spectra. The corresponding vertical profiles of horizontal reflectivity show very high values (above 55 dBZ) up to 3 km, then a steady decrease at a rate of  $1.5 \text{ dB km}^{-1}$ . The probability of hail derived from the classical comparison between the 45-dBZ height and the  $0^\circ\text{C}$  isotherm height is close to 1. Those facts strongly suggest that ice is present in the attenuating cells.

Ryzhkov et al. (2007), using an independent dataset (from the SIDPOL C-band radars from Alabama and Canada) and a somewhat similar methodology to estimate  $\gamma_{\text{DP}}$ , obtained very similar results and concluded that the differential attenuation hot spots were caused through resonant Mie scattering by a mixture of large raindrops and melting hail.

- Such hot spots can be identified by values of  $\rho_{\text{HV}}$  below 0.94, which, combined with high values of  $Z_{\text{H}}$ , can be considered a signature of the presence of wet ice. Such wet ice appears to be associated with high total and differential attenuation and also accompanied by high values of  $Z_{\text{DR}}$  and  $K_{\text{DP}}$ . If this is the case then we may have to question the suggestion that  $K_{\text{DP}}$  responds only to the presence of oblate raindrops and thus can provide accurate estimates of rainfall rates in the presence of hail.
- Among all the numerous intense convective cells ( $Z_{\text{H}} > 55 \text{ dBZ}$ ) that were analyzed in this work, only an extremely small percentage show the typical hail signature (low  $Z_{\text{DR}}$  and  $K_{\text{DP}}$ ). The conclusion surrounding that is that pure (dry) hail is very rare in the Paris area and that the dominant precipitation type in intense convective systems is wet ice, the forward and back-scattering of which are completely different from pure hail or pure rain.
- Operational correction of differential attenuation created by the so-called hot spots is clearly not a trivial task, especially if one considers that the accuracy of the correction has to be better than 0.1 dB for  $Z_{\text{DR}}$  to be usable in subsequent rainfall rate estimation and we cannot be confident of a simple link between  $\gamma_{\text{H}}$  and  $\gamma_{\text{DP}}$ . If the hydrometeors in the hot spots are indeed a mixture of rain drops and melting or wet ice then it will be very difficult to obtain a unique solution from the available polarization parameters for the sizes and shapes of both the rain drops and the wet ice particles. A more practical solution may be to flag any derived rain rates in such hot spots as error prone. It will also be very difficult to correct the ray profiles behind the hot spot for attenuation; in this case one strategy could be to use a second, probably more distant radar in the network, which is unlikely to suffer from hot spot attenuation in the same location.

*Acknowledgments.* The authors are indebted to Laurent Périer, Patrick Roquain, and Kim Do Khac from Météo France who developed the French CASTOR2 radar processor and made the polarimetric data collection possible. Julien Desplats (Météo France) kindly provided the seasonal statistics of rainfall accumulations for Paris and London.

## APPENDIX

**Derivation of the Uncertainty on the Estimated  $\gamma_{DP}$** 

We assume here for simplicity that the Bringi et al. (2001) relationship between intrinsic  $Z_H$  and  $Z_{DR}$  holds, that is,

$$Z_{DR,intrinsic} \text{ (dB)} = 0.048Z_{H,intrinsic} \text{ (dBZ)} - 0.774. \quad (\text{A1})$$

Second, we recall that the intrinsic  $Z_H$  ( $Z_{H,intrinsic}$ ) is recovered from the measured, possibly attenuated  $Z_H$  ( $Z_{H,measured}$ ) as follows:

$$Z_{H,intrinsic} = Z_{H,measured} + \gamma_H \phi_{DP}. \quad (\text{A2})$$

Finally, we recall that  $\gamma_{DP}$  is estimated as follows:

$$\gamma_{DP} = \frac{(Z_{DR,intrinsic} - Z_{DR,measured})}{\phi_{DP}}. \quad (\text{A3})$$

The true value of  $\gamma_H$  is not known and some value has to be assumed. If we denote by  $\Delta\gamma_H$  the difference between the true and the assumed values for  $\gamma_H$ , then, using Eq. (A2), it can be shown that it leads to an error on the estimated intrinsic  $Z_H$  ( $Z_{H,intrinsic}$ ) that is equal to

$$\Delta Z_{H,intrinsic} = \Delta\gamma_H \phi_{DP}. \quad (\text{A4})$$

Subsequently, via Eq. (A1), the error on the estimated intrinsic  $Z_{DR}$  ( $Z_{DR,intrinsic}$ ) is equal to

$$\Delta Z_{DR,intrinsic} = 0.048\Delta\gamma_H \phi_{DP}. \quad (\text{A5})$$

Finally, differentiating Eq. (A3) and injecting in it the above expression for  $\Delta Z_{DR,intrinsic}$  leads to the following expression for the uncertainty on  $\gamma_{DP}$ :

$$\Delta\gamma_{DP} = 0.048\Delta\gamma_H. \quad (\text{A6})$$

Most of all  $\gamma_H$  obtained by G06 lie within [0.07; 0.13]. With a mean value of  $0.1 \text{ dB}^{-1}$  for  $\gamma_H$ , this leads to a maximum error  $\Delta\gamma_H$  equal to 0.03 and in turn an error on  $\gamma_{DP}$  equal to  $0.00144 \text{ dB}^{-1}$ , which corresponds to a relative error around 5%.

## REFERENCES

- Brandes, E. A., G. Zhang, and J. Vivekanandan, 2002: Experiments in rainfall estimation with a polarimetric radar in a subtropical environment. *J. Appl. Meteor.*, **41**, 674–685.
- Bringi, V. N., and V. Chandrasekar, 2001: *Polarimetric Doppler Weather Radar: Principles and Applications*. Cambridge University Press, 636 pp.
- , T. D. Keenan, and V. Chandrasekar, 2001: Correcting C-band radar reflectivity and differential reflectivity data for rain attenuation: A self-consistent method with constraints. *IEEE Trans. Geosci. Remote Sens.*, **39**, 1906–1915.
- Carey, L. D., S. A. Rutledge, D. A. Ahijevych, and T. D. Keenan, 2000: Correcting propagation effects in C-band polarimetric radar observations of tropical convection using differential propagation phase. *J. Appl. Meteor.*, **39**, 1405–1433.
- Delobbe, L., and I. Holleman, 2006: Uncertainties in radar echo top heights used for hail detection. *Meteor. Appl.*, **13**, 361–374.
- Eilts, M., and Coauthors, 1996: Severe weather warning decision support system. Preprints, *18th Conf. on Severe Local Storms*, San Francisco, CA, Amer. Meteor. Soc., 536–540.
- Gourley, J. J., P. Tabary, and J. Parent du Chatelet, 2006a: Data quality of the Meteo-France C-band polarimetric radar. *J. Atmos. Oceanic Technol.*, **23**, 1340–1356.
- , —, and —, 2006b: Empirical estimation of attenuation from differential propagation phase measurements at C-band. *J. Appl. Meteor. Climatol.*, **46**, 306–317.
- , A. Illingworth, and P. Tabary, 2009: Absolute calibration of radar reflectivity using redundancy of the polarization observations and implied constraints on drop shapes. *J. Atmos. Oceanic Technol.*, **26**, 689–703.
- Hitschfeld, W., and J. Bordan, 1954: Errors inherent in the radar measurement of rainfall at attenuating wavelengths. *J. Meteor.*, **11**, 58–67.
- Jameson, A. R., 1992: The effect of temperature on attenuation-correction schemes in rain using polarization propagation differential phase shift. *J. Appl. Meteor.*, **31**, 1106–1118.
- Joe, P., D. Burgess, R. Pots, T. Keenan, G. Stumpf, and A. Treloar, 2004: The S2K severe weather detection algorithms and their performance. *Wea. Forecasting*, **19**, 43–63.
- Keenan, T. D., L. D. Carey, D. S. Zrnić, and P. T. May, 2001: Sensitivity of 5-cm wavelength polarimetric radar variables to raindrop axial ratio and drop size distribution. *J. Appl. Meteor.*, **40**, 526–545.
- Kozu, T., and K. Nakamura, 1991: Rainfall parameter estimation from dual-radar measurements combining reflectivity profile and path-integrated attenuation. *J. Atmos. Oceanic Technol.*, **8**, 259–270.
- Mishchenko, M. I., 2000: Calculation of the amplitude matrix for a nonspherical particle in a fixed orientation. *Appl. Opt.*, **39**, 1026–1031.
- Rasmussen, R. M., and A. J. Heymsfield, 1987: Melting and shedding of graupel and hail. Part I: Model physics. *J. Atmos. Sci.*, **44**, 2754–2763.
- Ryzhkov, A. V., 2007: The impact of beam broadening on the quality of radar polarimetric data. *J. Atmos. Oceanic Technol.*, **24**, 729–744.
- , and D. S. Zrnić, 1995: Precipitation and attenuation measurements at a 10-cm wavelength. *J. Appl. Meteor.*, **34**, 2121–2134.
- , P. Zhang, D. Hudak, J. L. Alford, M. Knight, and J. W. Conway, 2007: Validation of polarimetric methods for attenuation correction at C-band. Preprints, *33rd Conf. on Radar Meteorology*, Cairns, Australia, Amer. Meteor. Soc., P11B.12. [Available online at [http://ams.confex.com/ams/33Radar/techprogram/paper\\_123122.htm](http://ams.confex.com/ams/33Radar/techprogram/paper_123122.htm).]
- Smyth, T. J., and A. J. Illingworth, 1998: Correction for attenuation of radar reflectivity using polarisation data. *Quart. J. Roy. Meteor. Soc.*, **124**, 2393–2415.
- Tabary, P., A. Le Henaff, G. Vulpiani, J. Parent-du-Châtelet, and J. J. Gourley, 2006: Melting layer characterization and



- identification with a C-band dual-polarization radar: A long-term analysis. *Proc. Fourth European Radar Conf.*, Barcelona, Spain, ERAD, 17–20.
- Testud, J., E. Le Bouar, E. Obligis, and M. Ali-Mehenni, 2000: The rain profiling algorithm applied to polarimetric weather radar. *J. Atmos. Oceanic Technol.*, **17**, 332–356.
- Vulpiani, G., P. Tabary, J. Parent-du-Chatelet, and Frank S. Marzano, 2008: Comparison of advanced radar polarimetric techniques for operational attenuation correction at C band. *J. Atmos. Oceanic Technol.*, **25**, 1118–1135.
- Waldvogel, A., B. Federer, and P. Grimm, 1979: Criteria for the detection of hail cells. *J. Appl. Meteor.*, **18**, 1521–1525.
- Witt, A., M. D. Eilts, G. J. Stumpf, J. T. Johnson, E. D. Mitchelland, and K. W. Thomas, 1998: An enhanced hail detection algorithm for the WSR-88D. *Wea. Forecasting*, **13**, 286–303.